Journal for ImmunoTherapy of Cancer

Mutant calreticulin enables potent and selective CAR-T cell therapy in preclinical models of myeloproliferative neoplasms

Cecilia Pesini,[1,2,3,4] Mario Gil-Bellido,[1,5] Lorena S Millan,[1] Carmen Oñate,[1,3,4] Adanays Calvo-Pérez,[1,3,5] Llipsy Santiago,[1,2,6] Eldris Iglesias,[7] Jorge Paúl Bernal,[1,5] Miguel Araujo-Voces,[5] Laura Paz Artigas,[8] Laura García-Martínez,[7] Francisco J Roig,[7,9] Nieves Movilla Meno,[8] José Manuel Garcia-Aznar ,[8,10] Bárbara Menéndez-Jandula,[11] María Teresa Olave,[3,4,12,13] Gemma Azaceta Reinares,[3,4,13] Marta Garrote,[14,15,16] Alberto Alvarez-Larrán,[14,15] Eva M Gálvez,[2,3,17] Diego Sánchez Martínez,[3,4,5,18] Maykel A Arias,[1,2,5] Julian Pardo ,[1,2,3,4,5] Ariel Ramirez-Labrada [1,2,3,4]

To cite: Pesini C, Gil-Bellido M, S Millan L, *et al*. Mutant calreticulin enables potent and selective CAR-T cell therapy in preclinical models of myeloproliferative neoplasms. *Journal for ImmunoTherapy of Cancer* 2026;**14**:e012706. doi:10.1136/jitc-2025-012706

► Additional supplemental material is published online only. To view, please visit the journal online (https://doi.org/10.1136/jitc-2025-012706).

JP and AR-L are joint senior authors.

Accepted 25 November 2025

For numbered affiliations see end of article.

Correspondence to
Dr Ariel Ramirez-Labrada; aramirezlabrada@yahoo.es

Dr Julian Pardo; pardojim@unizar.es

ABSTRACT

Background The adoptive transfer of T cells engineered to express chimeric antigen receptors (CAR-T) has shown high efficacy and safety in treating various hematologic malignancies. However, many hematologic disorders, such as BCR::ABL1-negative myeloproliferative neoplasms (MPNs), lack effective treatment options. Some of these neoplasms are marked by a recurrent mutation that results in the expression of mutant calreticulin (mCALR), a neoantigen absent in healthy tissues, making it a highly specific and appealing target for CAR-T cell therapy.

Methods Five distinct CARs were designed based on available monoclonal antibody sequences that target mCALR and were subsequently used to generate CAR-T cells. The most effective construct was selected through functional in vitro assays against mCALR-positive cell lines. Its efficacy was then evaluated in cell lines, patient-derived cells, and orthotopic xenograft models, assessing tumor burden, CAR-T cell infiltration, and animal survival. Bulk and single-cell RNA sequencing were performed on patient-derived cells and residual tumor cells from CART-treated mice, respectively, to investigate potential resistance mechanisms. The impact of the most relevant pathway alteration on CAR-T efficacy was also analyzed. Pharmacological rescue assays using targeted agents were then conducted.

Results Among the five constructs, one demonstrated superior and specific cytotoxicity against mCALR-expressing cells, with no activity against mCALR-negative controls. This CAR-T cell also eliminated patient-derived MPN cells and controlled disease progression in xenograft models, which correlated with the persistence of CAR-T cells and tumor infiltration. Transcriptomic profiling of patient samples and residual tumor cells in spleens of treated mice revealed upregulation of anti-apoptotic proteins. Functional assays confirmed reduced CAR-T efficacy in Bcl-2 high cells, which was restored by co-treatment with venetoclax, indicating a viable combination approach to overcome resistance.

Conclusions This study demonstrates, for the first time, the successful targeting of mCALR with CAR-T cells as a therapeutic strategy for MPNs. The chosen construct shows strong preclinical efficacy against established cell lines and patient-derived cells. Additionally, transcriptomic profiling uncovered apoptosis resistance mechanisms and supports a combination strategy with BH3 mimetics, such as venetoclax. These findings

WHAT IS ALREADY KNOWN ON THIS TOPIC

⇒ CALR mutations generate a mutant-specific neoepitope (mCALR) restricted to malignant cells in BCR::ABL1 negative myeloproliferative neoplasms (MPNs). Despite its potential as a therapeutic target, chimeric antigen receptor (CAR)-based immunotherapeutic strategies to exploit this neoepitope have not yet been successfully developed.

WHAT THIS STUDY ADDS

⇒ This study provides the first preclinical validation of CAR-T cell therapy specifically targeting mCALR. The engineered CAR-T cells exhibited selective cytotoxicity against mCALR-expressing cells while sparing non-mCALR cells and demonstrated efficacy in two xenograft models as well as in primary samples from MPN patients.

HOW THIS STUDY MIGHT AFFECT RESEARCH, PRACTICE OR POLICY

⇒ These findings establish a proof of concept for targeting mCALR with CAR-T cells, opening the door to mutation-specific immunotherapies for MPNs. This approach could inform future strategies for early intervention in high-risk MPNs or for preventing disease progression.

provide a compelling rationale for ongoing preclinical development and future clinical application of anti-mCALR CAR-T cells for the treatment of MPNs.

INTRODUCTION

BCR::ABL1 negative myeloproliferative neoplasms (MPNs) are a heterogeneous group of clonal hematologic malignancies characterized by the overproduction of one or more myeloid lineages, typically driven by somatic mutations in multipotent hematopoietic stem cells. *JAK2*, *MPL*, or *CALR* mutations are associated with 85% of MPN cases. *CALR* mutations are a hallmark of essential thrombocythemia (ET) and primary myelofibrosis (MF), two major MPN subtypes. Currently, MF treatment is limited and remains an incurable disease, with a median survival of 6 years. ET is associated with better outcomes. However, *CALR*-mutated ET typically affects young patients who invariably evolve into MF in the long term, illustrating the urgent need for disease-modifying therapy in both MF and ET.[1 2]

CALR mutations are presented as insertions or deletions clustered within exon 9, resulting in a +1 base pair frameshift and the generation of a novel C-terminal tail, approximately 40 amino acids in length. Notably, while over 50 mutations have been described, all produce a similar neo-C-terminus, which can be classified into two predominant types: type 1, characterized by a 52-bp deletion, and type 2, characterized by a 5-bp insertion.[3–5] The resulting shared neoepitope has been recognized as a disease-specific antigen and a highly promising immunotherapeutic target.[6 7]

This novel C-terminal sequence results in the loss of the KDEL endoplasmic reticulum (ER) retention signal, altering the protein's localization and function.[4 8–10] The absence of the KDEL motif allows mutant calreticulin (mCALR) to enter the secretory pathway, leading to its aberrant localization in the trans-Golgi network and at the plasma membrane. mCALR aberrantly traffics to the cell surface via interaction with the thrombopoietin receptor (TPOR/MPL), initiating pathological signaling through activating the JAK/STAT pathway.[11] This process depends on specific glycan-binding domains, the N-terminal chaperone region, and the mutant-specific C-terminal tail.[11–15]

Current treatment strategies for MPNs remain limited, with unspecific JAK/STAT pathway inhibitors, such as ruxolitinib, offering only partial and transient responses. Allogeneic stem cell transplantation remains the only potentially curative therapy. However, it is associated with high toxicity and a mortality rate of 40% at 2 years in most series, making this procedure unsuitable for the majority of patients.[1 2 16–21] Therefore, there is an urgent unmet need for therapies targeting the disease at the molecular level, ideally during early transformation from the chronic to blast phase, while sparing healthy hematopoiesis.[22 23]

Despite the increasing development and approval of chimeric antigen receptor (CAR)-based therapies for hematological malignancies, their application to myeloid neoplasms remains limited, mainly due to the lack of truly tumor-specific antigens and the risk of on-target, off-tumor toxicity. In this context, the restricted expression of mCALR in specific cell subtypes and its critical role in disease pathogenesis provide a unique therapeutic opportunity for the development of CAR-T cell therapy, provided the approach is rigorously validated in preclinical models. The mCALR neoantigen represents a promising novel target. Although alternative strategies, such as peptide-based vaccines or blocking antibodies, have been explored, they have shown limited clinical efficacy to date, and adoptive cell therapies directed against this neoantigen remain undeveloped.[7 24 25]

This study aims to develop and functionally characterize a novel CAR-T cell therapy targeting the mCALR neoantigen in MPNs. Our approach is designed to leverage the disease-restricted expression of mCALR to achieve selective cytotoxicity against malignant cells while preserving healthy hematopoiesis. To this end, we engineered a CAR construct optimized for efficacy and safety and evaluated its performance through in vitro assays and in vivo xenograft models. We further investigated the capacity of these CAR-T cells to infiltrate disease-relevant tissues, assessed their persistence and functional activity, and explored potential resistance mechanisms and combinatory strategies to enhance therapeutic outcomes. This work sets the groundwork for translating mCALR-directed CAR-T cell therapy into the clinic as a targeted treatment for high-risk MPNs, including MF and prefibrotic ET.

RESULTS

Mutant calreticulin as a specific immunotarget for CAR-T cell therapy

Five second-generation CAR constructs were designed using the single-chain variable fragment (scFv) from the corresponding antibodies developed against mCALR with comparable kinetic and functional profiles (online supplemental table 1). Each consisted of the anti-mCALR scFv, a CD8 transmembrane spacer, and intracellular signaling domains from 4-1BB and CD3ζ. Constructs were cloned under the control of the EF1α promoter in T2A-based monocistronic (scFv-41BB-CD3ζ-T2A-eGFP) lentiviral vectors, which were linked to eGFP via a T2A sequence (figure 1A).

The expression of mCALR-CAR was confirmed by detecting surface scFv and eGFP expression in HEK-293T cells and primary T cells (online supplemental figure 1). Comparable transduction efficiencies were observed, as indicated by the percentage of GFP^+ cells (figure 1A). The five constructs were subsequently tested in vitro using tumor cell-killing assays. To evaluate CAR-T cell functionality and selectivity, we employed myeloid cancer cell lines that do not naturally express mCALR, alongside isogenic counterparts engineered to overexpress the antigen. This controlled system allowed us to directly compare CAR-T

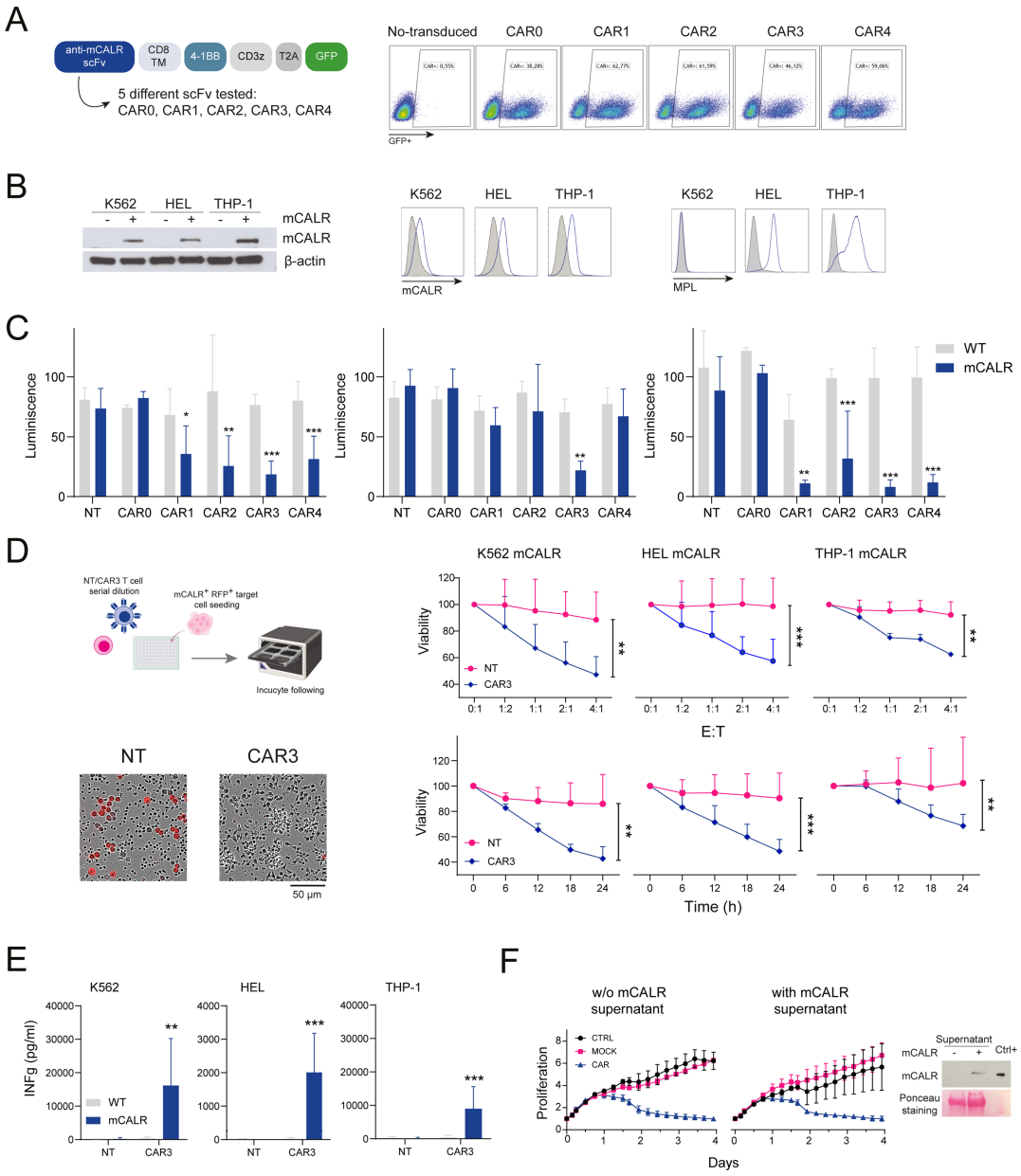

Figure 1 Development and in vitro characterization of an anti-mutant calreticulin (mCALR) CAR T-cell therapy. (A) Left panel: schematic illustration of the five CAR constructs evaluated. Right panel: representative flow cytometry dot plots showing efficient transduction of primary T cells, as indicated by GFP expression. (B) Left panel: western blot analysis confirming overexpression of mCALR in engineered K562, HEL, and THP-1 cell lines. β-actin served as a loading control. Right panel: flow cytometric assessment of surface mCALR and MPL expression in engineered cell lines. Gray histograms correspond to controls (secondary antibody only for mCALR and isotype control for MPL), while blue histograms represent specific staining. (C) Initial cytotoxicity screening of the five CAR constructs against wild-type (WT, gray) and mCALR-expressing (mCALR, blue) K562, HEL, and THP-1 cells, all expressing luciferase, assessed by luminescence relative to control wells without effector cells at an effector-to-target (E:T) ratio of 4:1 after 48 hours. Statistical differences were analyzed by comparing each CAR construct in mutant CALR cells to the wild-type cell line (CAR0 n=2; NT, CAR3, n=3; CAR1, CAR2, CAR4 n=4). (D) Top left panel: schematic illustration of the protocol followed for cytotoxicity of the selected CAR3 construct against RFP$^+$ mCALR$^+$ monitored by Incucyte real-time imaging. Top right panel: cytotoxicity analysis of the selected CAR3 construct at multiple E:T ratios at 24 hours against the indicated cell lines (n=3). Bottom left panel: representative Incucyte image showing cytotoxicity at an E:T ratio of 8:1, bottom right panel: cytotoxicity kinetics over 24 hours at 8:1 E:T (n=3). Target cell viability was calculated based on the red-shaded area, representing confluence normalized to time zero and to control wells without effector cells. Non-transduced (NT, pink) and CART3-mCALR-transduced (blue) T cells were compared. (E) IFN-γ secretion in culture supernatants after 24-hour co-culture of NT and CART3-mCALR cells with WT (gray) or mutant mCALR (blue) K562, HEL, and THP-1 cells at a 4:1 E:T ratio, as determined by ELISA (n=3). (F) Right panel: time-course cytotoxicity against HEL mCALR cells of NT (pink) or CART3-mCALR (blue) cells, and controls without effector cells (black), in the presence or absence of supernatant with mCALR (n=3). Left panel: western blot of cell culture supernatants verifying soluble mCALR production. Data are presented as mean±SD. *p<0.05, **p<0.01, ***p<0.001 by Student's t-test.

cell activity in the presence or absence of mCALR within an identical genetic and cellular background.

As previously suggested, mCALR expression can signal independently of MPL.[26 27] To investigate whether CAR-T cells can recognize and kill mCALR-expressing cells regardless of MPL expression, we selected myeloid cell lines with different MPL expression statuses. Specifically, we used the CML-derived erythroleukemia cell line K562 (MPL$^-$, mCALR$^-$) and the AML cell lines HEL (MPL$^+$, mCALR$^-$) and THP-1 (MPL$^+$, mCALR$^-$), along with their respective mCALR$^+$ overexpressing derivatives, all of which showed no differences in proliferation rate (online supplemental figure 2). Western blot analyses confirmed mCALR expression in the transfected sublines (figure 1B), and its localization at the plasma membrane was further validated by flow cytometry. Notably, mCALR was detected in the cell membrane of K562 cells that do not express MPL (figure 1B), confirming previous functional studies using other myeloid cell lines like MARIMO[27] and *C. elegans* model.[26]

Subsequently, we found that four out of five CART-mCALR cells specifically eliminated mCALR$^+$ cells compared with control mCALR$^-$ cells (figure 1C), confirming that expression of mCALR in the cell membrane renders tumor cells susceptible to targeting with CART-mCALR cells. Although the percentage of CAR-T cell populations was normalized to enable a fair comparison of cytotoxic activity between constructs, the cytotoxic potential varied across different cell lines, with CART3-mCALR demonstrating the most significant and consistent cytotoxicity among the constructs tested. In addition, cytokine secretion was evaluated, revealing that CART3-mCALR induced the highest levels of IL-2, TNFα, MIP-1α, and MIP-1β, identifying it as the most functionally active construct (online supplemental figure 3).

Based on these results, we selected CART3-mCALR for further studies because it demonstrated the highest efficacy. First, we thoroughly analyzed the effectiveness of CART3-mCALR using various effector-to-target (E:T) ratios and time points, comparing CAR-expressing and non-transduced T cells through IncuCyte-based cytotoxicity assays. This confirmed that CART3-mCALR-mediated cytotoxicity depended on both time and ratio, exhibiting a characteristic cytotoxicity profile and thus confirming the CART's effectiveness (figure 1D). This effect was also confirmed against mCALR type 1, type 2, and the MARIMO mutant CALR variant (online supplemental figure 4). In addition, the lack of cytotoxicity against tumor cell lines of different origins, as well as primary cells, indicates good selectivity toward mCALR-expressing cells, supporting its safety (online supplemental figures 5 and 6). CART3-mCALR also produced high levels of the proinflammatory cytokine IFN-γ when co-cultured with mCALR$^+$ cell lines, confirming their cytotoxic activity (figure 1E). As previously found using a single E:T ratio and time point, we did not observe differences in cytotoxicity based on MPL expression; both MPL-positive (HEL and THP-1) and MPL-negative (K562) cell lines were equally sensitive to CART3-mCALR cells at all E:T ratios and time points tested.

In addition to being expressed on the plasma cell membrane, mCALR$^+$ cell lines also secreted mCALR into the cell culture supernatants (figure 1F) as previously described,[28] which could affect CAR-T cell activity. However, cell cytotoxicity mediated by CART3-mCALR was not diminished when using a medium enriched with soluble mCALR (smCALR), indicating that it remains active even in a smCALR-enriched environment (figure 1F). This finding is consistent with previous studies showing that smCALR is secreted bound to transferrin receptor 1 (sTFR1) or sequestered by albumin, potentially blocking CAR scFv binding and preventing inhibitory effects.[28]

CART3-mCALR exerts a strong antitumor effect in vivo in the HEL mCALR$^+$ mouse xenograft model

We next evaluated the therapeutic efficacy of CART3-mCALR in vivo in twelve NOD.CB17-Prkdcscid IL2rgtm1/BcgenHsd (B-NDG) mice (n=6 per group, mock and treated) engrafted with luciferase-expressing HEL mCALR$^+$ cells (figure 2A). Engraftment was confirmed through bioluminescent imaging (BLI) before treating the mice. compared with eGFP mock transduced T cells, treatment with CART3-mCALR cells (eGFP or CAR expression 40%=2×10^6 cells) resulted in long-term survival for most of the mice (except one, mouse #4, which died due to xeno-GVHD), indicating a high efficacy in vivo for treating mCALR$^+$ tumors (figure 2B). The mCALR$^+$ cell burden in mice treated with CART3-mCALR cells decreased during the first week of treatment compared with those receiving mock T cells, and this difference persisted throughout the experiment (figure 2B). Additionally, flow cytometry analysis of peripheral blood obtained from submandibular vein bleeding on day 21 after CAR-T cell treatment revealed a significant expansion of CART3-mCALR cells in CAR-T-treated mice compared with those treated with mock cells (figure 2C), consistent with antigen-specific stimulation in vivo, which is known to be critical for the therapeutic efficacy of CAR-T cells. One mouse treated with CAR-T cells was humanely euthanized due to signs consistent with xenogeneic graft-versus-host disease (xGVHD, 79% human T cells relative to total cells in peripheral blood at euthanization, 80% in bone marrow and 97% in spleen), a known complication in humanized mouse models characterized by robust human T cell activation. This observation highlights our system's effective human immune cell engraftment and aligns with previous reports of xGVHD in comparable settings.

A significantly higher tumor burden in the spleen and liver, as quantified by BLI, was observed in mock-treated mice compared with those treated with CART3-mCALR cells after euthanasia. These findings suggest that CART3-mCALR cells effectively eliminate mCALR$^+$ cells and reduce metastatic spread. This was further supported by the quantification of an apparent reduction in CD33$^+$

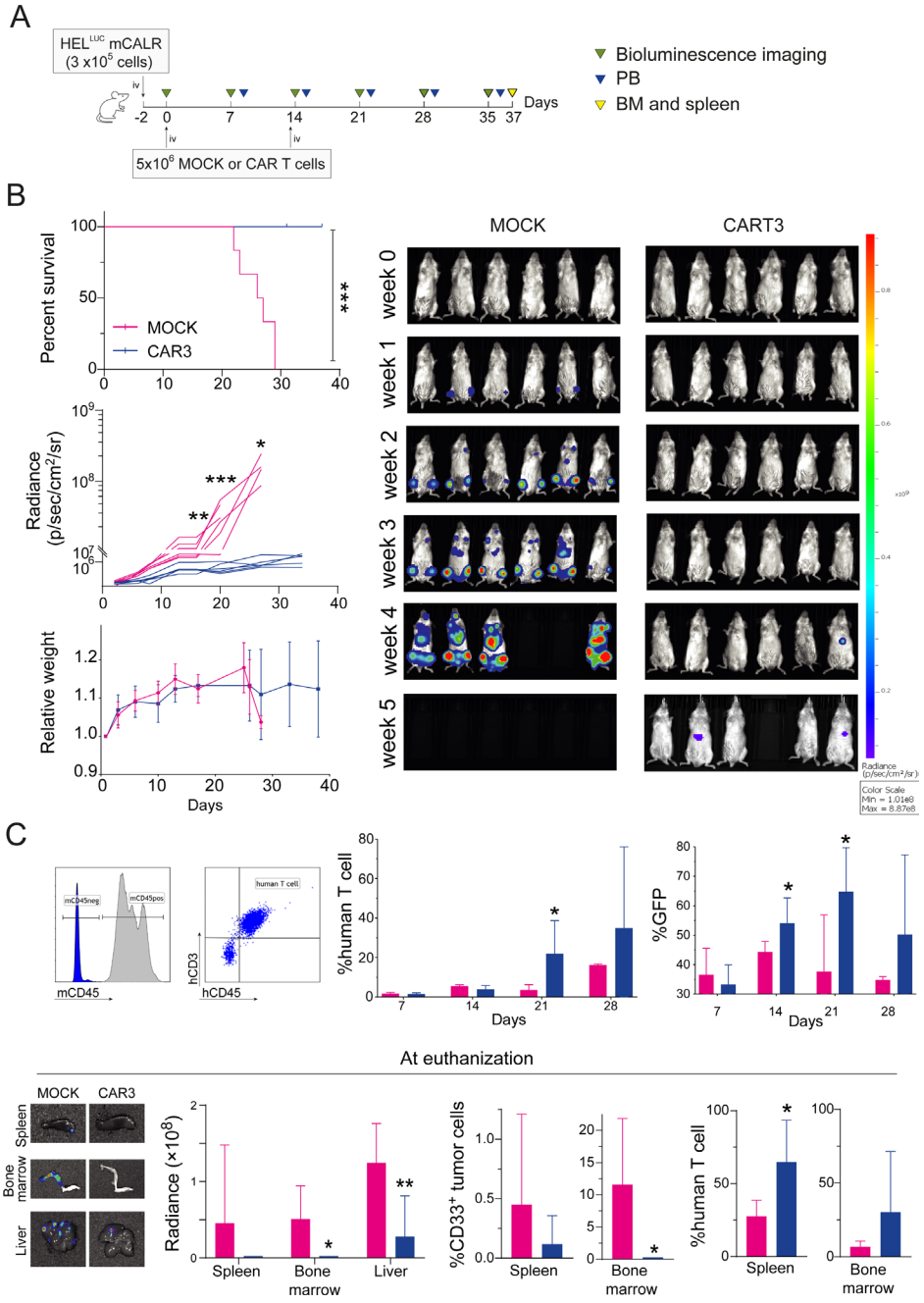

Figure 2 In vivo antitumor efficacy of CART3-mCALR cells. (A) Experimental timeline of the cell line-derived xenograft model in B-NDG mice (n=6 per group). Mice were intravenously injected with HEL mCALR$^+$ cells expressing luciferase, followed by infusion of GFP-transduced (MOCK) or CART3-mCALR cells. (B) Top left panel: Kaplan-Meier survival curves comparing MOCK (pink) and CART3-mCALR (blue) T cell-treated groups. Survival differences were analyzed using the log-rank test. Mice were regularly monitored for weight loss or the development of hind limb paralysis. Euthanasia was performed if mice lost ≥20% of their body weight or developed paralysis. Middle left panel: quantification of average bioluminescent radiance (p/s/cm^2/sr) per mouse at the indicated time points. Bottom left panel: relative body weight of mice monitored throughout the study. Values are normalized to baseline weight. Right panel: representative bioluminescent images showing tumor progression over time per group. (C) Upper panel left: Representative gating strategy and detection of human T cells in peripheral blood (PB) by flow cytometry. Histogram showing the discrimination between mouse CD45$^+$ cells and CD45$^-$ events, from which human T cells (hCD45$^+$ hCD3$^+$) are selected. Bar graphs showing human T cells (middle) and GFP$^+$ or CART3-mCALR$^+$ cells (GFP$^+$: hCD45$^+$ hCD3$^+$ GFP$^+$, CAR, right) at the indicated time points. Lower panel: tumor burden at the time of sacrifice (MOCK: days 22, 23, 26, 27, 29, and 29; CAR: day 37 at study endpoint, except one mouse sacrificed on day 31 for humane reasons due to GVHD) in the indicated organs by ex vivo BLI (average radiance, left) and flow cytometry (CD33$^+$ ZsGreen$^+$ cells, middle). Right: infiltrating human T cells by flow cytometry in the spleen and bone marrow (BM) at the time of euthanasia. Data are presented as mean±SD. Statistical significance was determined using unpaired two-tailed Student's t-test (*p<0.05, **p<0.01, ***p<0.001), comparing each CART3-mCALR-treatment condition to its matched MOCK control. GVHD, graft-versus-host disease; mCALR, mutant calreticulin.

(mCALR$^+$) tumor cells in the spleen and bone marrow of CAR-T-treated mice detected by flow cytometry. However, it only reached statistical significance in the bone marrow (figure 2C).

Additionally, after euthanasia, higher numbers of human T lymphocytes were detected in the spleens and bone marrows of mice treated with CART3-mCALR cells. However, statistical significance was achieved only in the spleens (figure 2C). This finding is suggested to be relevant, given that the bone marrow is the primary site of malignant clone emergence in MPNs, and the effective homing of adoptively transferred T cells to this compartment is crucial for sustained therapeutic efficacy. Alongside the spleen, the bone marrow also acts as a key reservoir for clonal expansion during disease progression and as a niche for therapy-resistant clones. These results further support the ability of CART3-mCALR cells to migrate, accumulate, and selectively eliminate target cells in both the bone marrow and spleen.

CART3-mCALR effectively eliminates MPL-negative tumors with low endogenous mCALR expression

To further validate our observations, we assessed the cytotoxic potential of CART3-mCALR cells using MARIMO cells, which, to our knowledge, represent the only established cell line that naturally expresses mCALR. This provides a more faithful model that closely resembles physiological mCALR expression. This cell line, reported to lack MPL expression, was derived from a patient with ET who progressed to secondary acute myeloid leukemia (sAML).[8 9] Notably, although the surface expression of mCALR has been shown to depend on MPL,[11] MARIMO cells retain a functional mCALR pathway independently of MPL.[26 27] We first confirmed that MARIMO cells do not express MPL (figure 3A) and found that the expression of mCALR is lower than in transfected cells (online supplemental figure 7). Despite low mCALR expression, CART3-mCALR cells efficiently eliminated parental MARIMO cells, while mCALR KO cells were spared, similar to control NT cells, with no statistically significant differences between them (figure 3A and online supplemental figure 7), demonstrating that cytotoxicity specifically depends on mCALR expression. This finding, consistent with results obtained in K562, THP-1, and HEL cells, is particularly compelling as it was observed in MARIMO cells, a more stringent and physiologically relevant model that naturally expresses mCALR.

These findings were further validated in vivo using an immunodeficient xenograft model in B-NDG mice (n=10; five per group, mock and treated). As previously conducted in the HEL mCALR$^+$ model (figure 2), mice were treated 2 days later with either eGFP (mock) or CART3-mCALR cells, accounting for 40% of the infused T-cell population (2×10^6 cells) (figure 3B). Mice receiving mock T cells reached humane endpoints within the first 3 weeks due to disease progression, while those treated with CART3-mCALR cells exhibited sustained tumor control (figure 3C). Weekly BLI revealed a marked reduction in tumor burden beginning in the third week post-treatment in the CAR-treated group, with 1 out of 5 mice showing complete tumor regression. As a health proxy, body weight followed an inverse trend relative to tumor load, with CART3-mCALR-treated mice maintaining weight more effectively than controls. Flow cytometry analysis of peripheral blood confirmed these findings, showing a significant reduction in CD33$^+$ ZsGreen$^+$ tumor cells at day 20 (figure 3D). In parallel, there was a 10-fold expansion of circulating T cells from week 2 to week 3, with CART3-mCALR (hCD3$^+$GFP$^+$) cells constituting up to 80% of the T cell population. These data demonstrate an inverse correlation trend between CAR-T cell expansion and tumor burden.

To compare tumor burden, T-cell trafficking, and CAR-T cell expansion and persistence between mock and treated cohorts, samples were collected and analyzed as mice reached their humane endpoints. 2 weeks after the last mouse in the mock cohort had reached its humane endpoint, all surviving mice in the CART3-mCALR–treated group were euthanized to harvest tissues for analyses. At this time point, CART3-mCALR cell-treated mice exhibited a significant reduction in tumor burden compared with mock-treated animals, achieving complete tumor clearance in one mouse and demonstrating a strong trend toward increased infiltration of human T lymphocytes in both the spleen and bone marrow (figure 3D). To assess long-term disease control and CAR-T cell persistence under milder tumor pressure, an additional in vivo experiment was performed using a lower number of injected MARIMO cells and a reduced CAR-T cell dose. This experimental setting, which allowed the evaluation of overall survival and sustained antitumor protection—including anti-relapse efficacy—over an extended follow-up period, demonstrated that CAR-T cells provide long-term survival benefits and prevent relapse in mice bearing MARIRO cell line tumors (online supplemental figure 8). These results highlight the in vivo efficacy of CART3-mCALR, including in MARIMO cells, the only cell model known to naturally express mCALR, and the capacity of CART3-mCALR cells to target mCALR-expressing malignant clones within immunoregulatory niches, such as the bone marrow and spleen, underscoring the importance of CAR-T cell expansion for effective tumor control.

These results validate the overall in vivo efficacy of CART3-mCALR. Nonetheless, compared with the mCALR-overexpression model (figure 2), efficacy in the high-dose MARIMO model was lower, with only one CAR-T-treated mouse dying before the experimental endpoint, likely reflecting the greater aggressiveness of MARIMO-driven disease and indicating that the therapeutic effects observed here occur under stringent, physiologically mCALR expression-relevant conditions characterized by low endogenous mCALR expression.

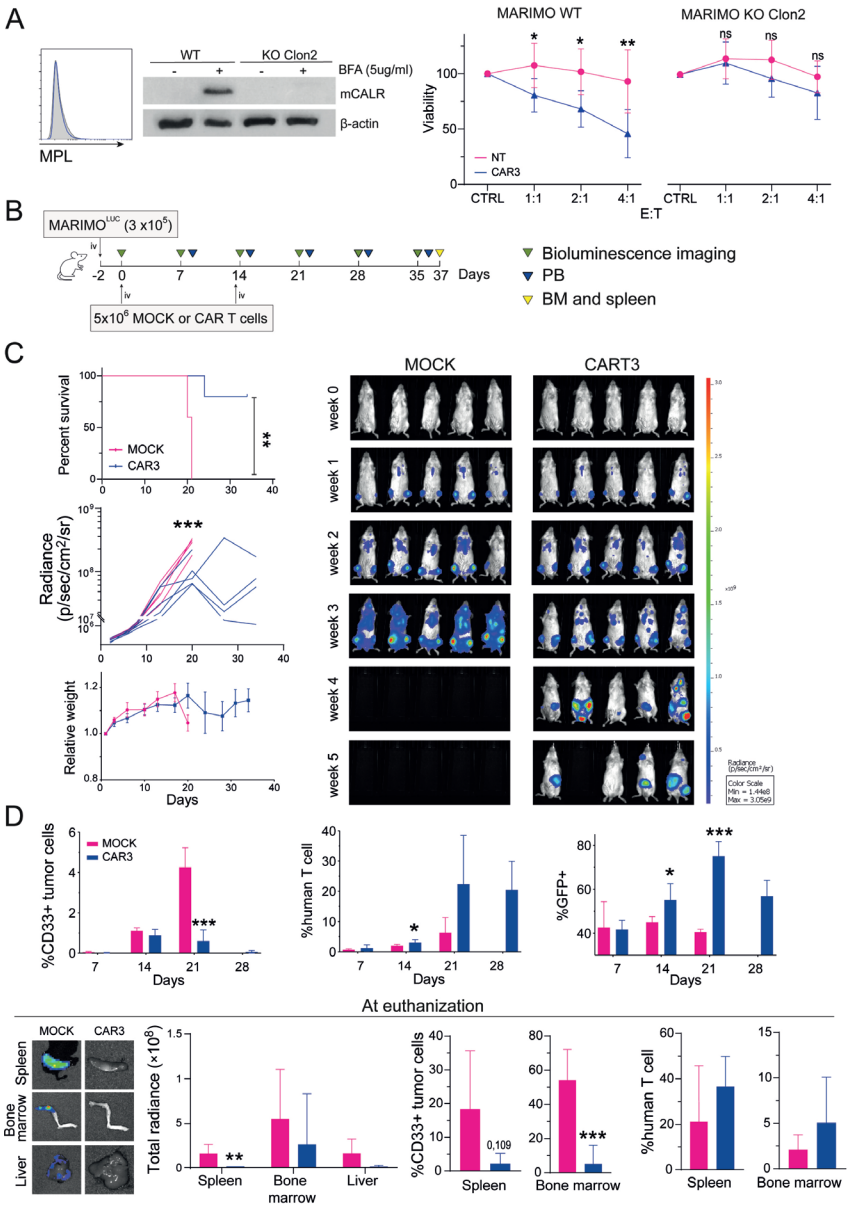

Figure 3 In vitro and in vivo antitumor efficacy of CART3-mCALR cells against the low mCALR-expressing MARIMO cell line. (A) Flow cytometry analysis of surface MPL expression in MARIMO cell lines. Gray histograms represent isotype controls; blue histograms indicate specific staining. Middle panel: western blot showing endogenous mCALR expression in wild-type MARIMO cells and confirmation of mCALR knockout (KO) generation. Cells were pretreated with brefeldin A (BFA) to enhance detection. β-actin served as a loading control. Right: in vitro cytotoxicity assay using wild-type and mCALR KO MARIMO clone 2 at various E:T ratios, assessed by luminescence relative to control wells without effector cells. Non-transduced (NT, pink) and CART3-mCALR-transduced (blue) cells were compared. (B) Experimental timeline of the cell line-derived xenograft model in B-NDG mice (n=5 per group) intravenously injected with MARIMO cells expressing luciferase, followed by infusion of GFP-transduced (MOCK) or CART3-mCALR cells. (C) Top left panel: Kaplan-Meier survival curves of mice treated with MOCK (pink) or CART3-mCALR-treated (blue) groups. Survival differences were analyzed using the log-rank test. Mice were regularly monitored for weight loss or the development of hind limb paralysis. Euthanasia was performed if mice lost ≥20% of their body weight or developed paralysis. Middle left panel: quantification of average bioluminescent radiance (p/s/cm^2/sr) per mouse at the indicated time points. Bottom left panel: relative body weight of mice monitored throughout the experiment. Values are normalized to baseline weight. Right panel: representative bioluminescent images showing tumor progression over time per group. (D) Upper panel: detection of tumor burden (CD33$^+$ ZsGreen$^+$), human T cells (hCD45$^+$ hCD3$^+$, middle), and GFP$^+$ or CART3-mCALR$^+$ cells (GFP$^+$: hCD45$^+$ hCD3$^+$ GFP$^+$, right) in peripheral blood by flow cytometry at the indicated time points over time. Lower panel: tumor burden at the time of sacrifice (MOCK: days 20, 20, 21, 21, and 21; CAR: days 24, 35, 35, 35, and 35 at study endpoint) in the indicated organs by ex vivo BLI (average radiance, left) and by flow cytometry (CD33$^+$ ZsGreen$^+$ cells, middle). Right: infiltrating human T cells by flow cytometry in spleen and bone marrow (BM) at the time of euthanasia. Data are presented as mean±SD. Statistical significance was determined using unpaired two-tailed Student's t-test (*p<0.05, **p<0.01, ***p<0.001), comparing each CART3-mCALR-treatment condition to its matched MOCK control. E:T, effector-to-target; mCALR, mutant calreticulin.

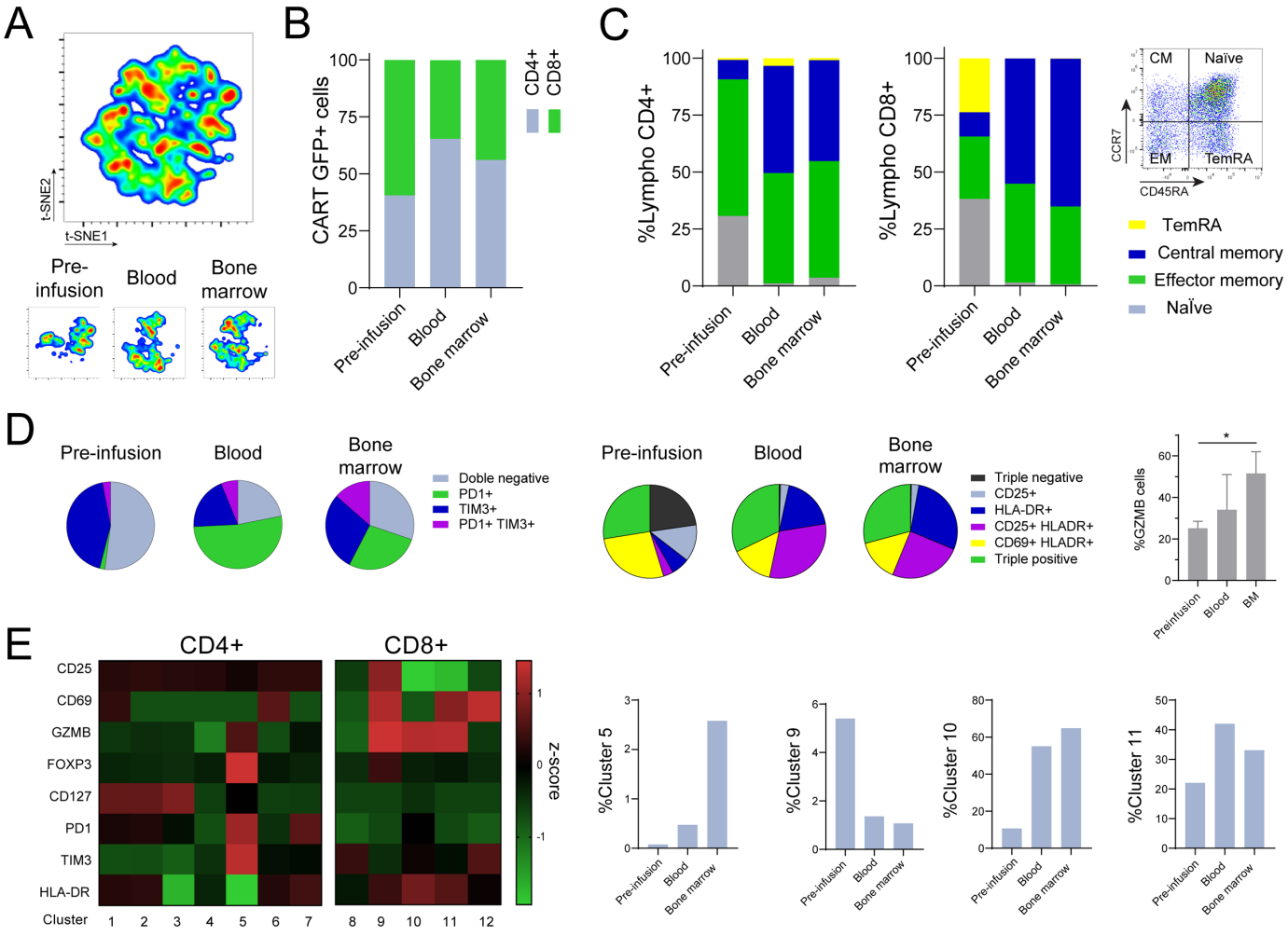

Figure 4 CART3-mCALR cell phenotypic remodeling, expansion, and activation in vivo. (A) Unsupervised t-SNE projection of CAR3-mCALR-expressing T cells (hCD45$^+$ hCD3$^+$ GFP$^+$) pre-mice infusion (preinfusion) and at the time of sacrifice recovered from blood and bone marrow. (B) Percentage of CD4$^+$ and CD8$^+$ subsets within CART3-mCALR cells preinfusion and recovered from blood and bone marrow. (C) Left panel: phenotypic composition of CART3-mCALR cells within CD4$^+$ and CD8$^+$ subsets, respectively, based on CD45RA and CCR7 expression, pre-infusion, and in blood and bone marrow. Right panel: representative dot plot. Naïve (CD45RA$^+$ CCR7$^+$, gray), central memory (CD45RA$^+$ CCR7$^+$, blue), effector memory (CD45RA$^-$ CCR7$^-$, green), and TemRA (CD45RA$^+$ CCR7$^-$, yellow). (D) Distribution of CART3-mCALR cells by exhaustion marker expression (PD1, TIM3, left panel), by activation marker expression (CD69, CD25, and HLA-DR, middle panel) and by granzyme B (GZMB, right bar graph) expression in CAR-T cells in preinfusion and postinfusion in blood and bone marrow. Data are presented as mean±SD. (E) Left: heatmap showing the 12 FlowSOM-identified clusters based on differentiation, activation, and functional marker expression (CD25, CD69, GZMB, FOXP3, CD127, PD1, TIM3, HLD-DR). CD4$^+$ (1–7 clusters) is shown on the left, CD8$^+$ (8–12 clusters) on the right. Red indicates higher expression, green lower expression. Right, frequency of cluster 5 (CD4$^+$ CD25$^+$ FoxP3$^+$ TIM3$^+$ PD1$^+$ GzmB$^+$), cluster 9 (CD8$^+$ CD25$^+$, FoxP3$^+$, CD69$^+$, GzmB$^+$), cluster 10 (CD8$^+$ HLA-DR$^+$ GzmB$^+$ PD1$^-$ TIM3$^-$) and cluster 11 (CD8$^+$ CD69$^+$ HLA-DR$^+$ GzmB$^+$ PD1$^-$ TIM3^{low}). mCALR, mutant calreticulin.

Expansion of memory CART3-mCALR cells accompanies in vivo persistence and antitumor activity

Given the critical role of CAR-T cell expansion and phenotypic composition in clearing tumor cells, we conducted an in-depth analysis of CAR-T cell populations before and after in vivo expansion, using cells recovered from blood and bone marrow at the time of sacrifice. Unsupervised flow cytometry analysis was performed on preinfusion and postinfusion CAR-T cells based on the expression of 14 surface markers associated with distinct differentiation states, activation status, and effector function (figure 4A). Since no differences were seen in the dimensionality reduction and clustering maps (t-SNE) of CART3-mCALR cells from mice engrafted with either HEL mCALR+ or MARIMO cells, all samples were combined into a single cohort for further analysis (online supplemental figure 9).

At the time of injection, about 60% of the CART3-mCALR cell population was composed of CD8$^+$ T cells (figure 4B), which aligns with previously reported ranges.[29] However, following in vivo inoculation, CD4$^+$ T cells expanded more significantly, increasing from 40% to about 60% of the CAR-T cell pool in peripheral blood and bone marrow by the endpoint. CART3-mCALR cells exhibited a heterogeneous distribution of differentiation states prior to injection. In CD4$^+$ CAR-T cells, the

predominant subsets were naïve (CD45RA$^+$ CCR7$^+$) and effector memory (CD45RA$^-$ CCR7$^-$). In contrast, CD8$^+$ CAR-T cells included not only naïve and effector memory phenotypes but also central memory (CD45RA$^-$ CCR7$^+$) and terminal effector memory RA-positive (TemRA; CD45RA$^+$ CCR7$^-$) subsets (figure 4C).

Following retrieval from bone marrow and peripheral blood at the time of sacrifice, CAR-T cells exhibited clear phenotypic remodeling. Naïve and TemRA subsets were nearly undetectable within the CD4$^+$ and CD8$^+$ compartments. In contrast, central memory and effector memory subsets were markedly enriched across both T cell populations (figure 4C). This phenotypic shift suggests that CART3-mCALR cells underwent in vivo activation and differentiation, creating a robust effector response while progressively losing less differentiated and terminally differentiated subsets on tumor engagement. The expansion of central memory cells supports the notion of sustained CAR-T cell persistence, likely contributing to long-term antitumor surveillance.

This phenotypic shift became more evident when analyzing exhaustion and activation markers (figure 4D). Specifically, we observed a marked increase in the proportion of CART3-mCALR cells co-expressing PD1 and TIM3 and a general rise in PD1$^+$ cells. In parallel, we detected an elevated expression of activation markers, particularly those associated with sustained activation, such as CD25 and HLA-DR (figure 4D). These phenotypic changes reflect the functional activation and in vivo expansion of CAR-T cells, with differentiation toward more mature and functionally competent subsets. While the emergence of exhaustion markers may indicate early stages of functional decline in some populations.[30 31] The persistence of a GzmB$^+$ fraction suggests that functional CAR-T cells remain capable of sustaining antitumor activity.

A more detailed FlowSOM analysis revealed 12 phenotypically distinct populations, seven within the CD4$^+$ compartment and five within the CD8$^+$ compartment (figure 4E). Among CD4$^+$ cells, a notable subset exhibited a Treg-like phenotype (CD25$^+$, FoxP3$^+$, TIM3$^+$, PD1$^+$) expressing GzmB. Although relatively rare, this population showed increased representation in the bone marrow. Within the CD8$^+$ compartment, we identified a population (CD25$^+$, FoxP3$^+$, CD69$^+$, GzmB$^+$) present in the infused CAR-T cells that was no longer detectable in vivo. In contrast, postinfusion, the most expanded CD8$^+$ populations included two subsets characterized by a sustained activation state (HLA-DR$^+$, GzmB$^+$, PD1$^-$, TIM3^{low}), confirming the predominant cytotoxic role of CD8$^+$ CAR-T cells compared with the helper/regulatory profile of CD4$^+$ CAR-T cells, as also observed in our in vitro assays using purified CD4$^+$ and CD8$^+$ CART3-mCALR cells (online supplemental figure 10).

This shift toward an activated phenotype, along with the presence of central memory and effector memory subsets, is associated with long-lasting immune protection, enhanced therapeutic efficacy, and improved CAR-T cell persistence.[32 33]

Autologous CART3-mCALR cells derived from MPN patients exhibit potent antitumor activity against aberrant clones

Given the known T cell dysfunctions in patients with MPNs and the potential impact of prior therapies, such as ruxolitinib or chemotherapy, on T cell fitness and function, we aimed to determine whether T cells from these patients could be utilized as an effective CAR-T therapy. To evaluate the feasibility and efficacy of generating functional CART3-mCALR cells from patients with MPNs, we transduced T cells from HDs and patients using the mCALR-CAR3 construct (figure 5A). Flow cytometry analysis revealed a similar 25-fold expansion and efficient transduction in both groups, with comparable CAR expression levels (over 50%) at day 5 postactivation (figure 5B,C). No significant differences were observed between the two sources, indicating that CAR-T cells from HDs and patients expanded effectively in vitro. Moreover, both CAR-T cells displayed similar activation profiles, as evidenced by the upregulation of canonical markers such as CD25, PD1, and GzmB (figure 5C).

Next, we evaluated their cytolytic capacity using HEL mCALR+ cells. Both HD-derived and patient-derived CART3-mCALR cells exhibited robust and comparable cytotoxic activity at 24 and 48 hours against these target cells, with no significant differences noted between the two groups (figure 5D).

Finally, we expanded this analysis using an autologous system to evaluate the ability of CART3-mCALR cells to eliminate primary malignant CD34$^+$ cells isolated from the peripheral blood of patients (online supplemental table 2). CAR-T cells derived from patients with MPN were equally effective as those generated from HDs in eradicating patient-derived CD34$^+$ aberrant cells (figure 5E). No statistically significant differences in killing efficacy were observed between autologous and allogeneic CAR-T cells, highlighting the therapeutic potential of using patient-derived T cells for targeted immunotherapy against mCALR$^+$ clones.

This finding is particularly relevant given prior reports suggesting that disease progression in MPNs may be associated with T-cell dysfunction due to altered cytokine profiles, which can compromise cytotoxic responses. Our results demonstrate that, despite potential immune dysregulation in these patients, their T cells retain sufficient functional capacity to be reprogrammed into potent CAR-T cells.

BH3-mimetics maximize CART3-mCALR cell-antitumoral efficacy

Disease relapse after CAR-T cell therapy occurs in up to 50% of treated patients. Understanding antigen-independent resistance mechanisms that impair CAR-T cell cytotoxicity and identifying patients at higher risk of relapse is essential for enhancing therapeutic efficacy and long-term outcomes. To identify potentially dysregulated pathways in MPNs, we conducted transcriptomic analysis through bulk RNA sequencing on magnetic bead-purified hematopoietic stem and progenitor cells

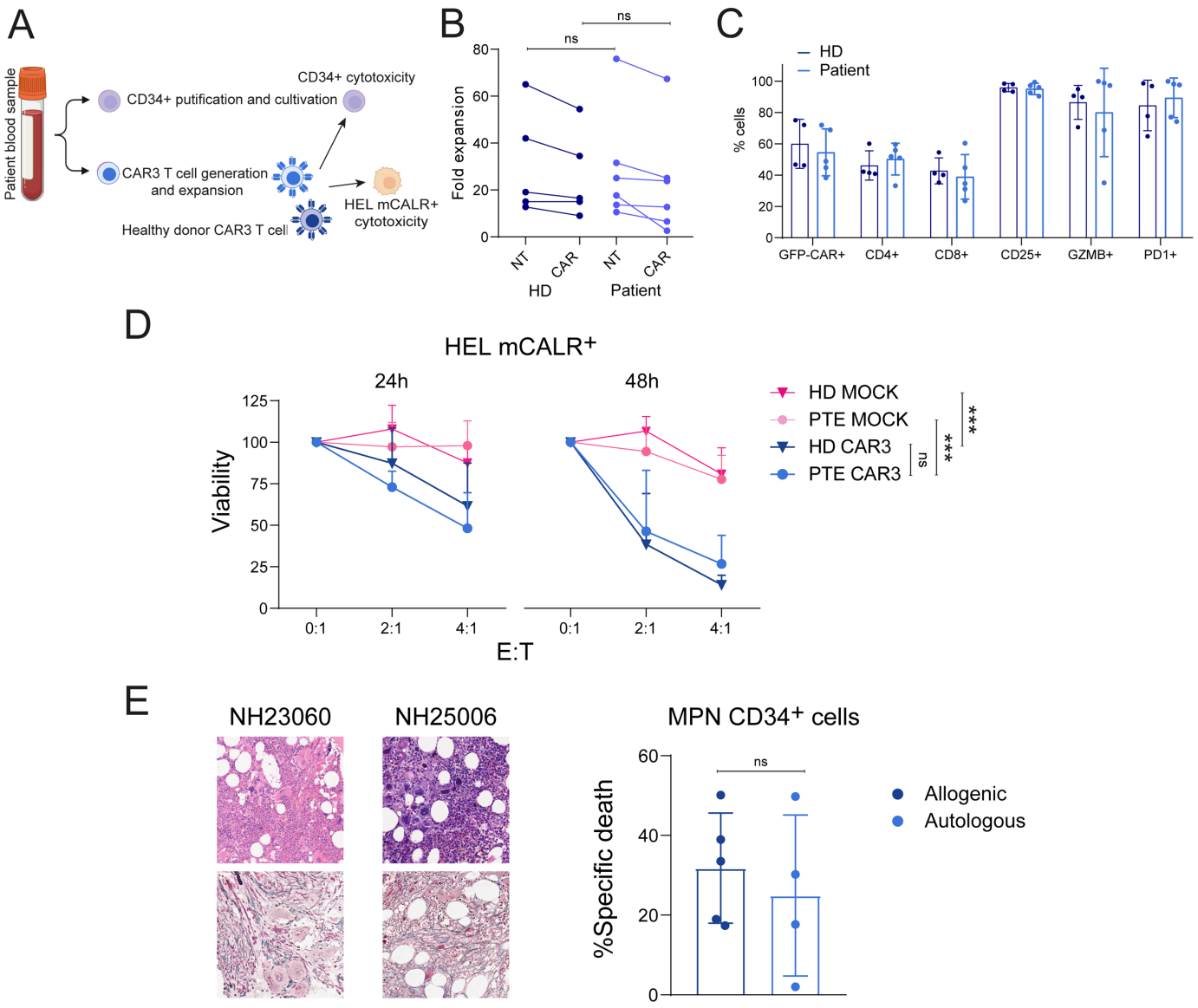

Figure 5 Efficient generation and antitumor activity of autologous CART3-mCALR cells from patients with MPNs. (A) Schematic workflow illustrating the purification of CD34$^+$ cells from peripheral blood samples of patients with MPN and the generation of autologous CART3-mCALR cells from CD34$^-$ fractions. Cytotoxic activity was subsequently evaluated against HEL mCALR cells and patient-derived CD34$^+$ malignant cells. (B) Fold expansion of CART3-mCALR cells from HD and patients at day 5 postactivation (n=6). (C) Flow cytometry analysis of CART3-mCALR cells derived from HD (n=5) and patients (n=4) at day 5 post-transduction showing percentage of GFP$^+$ (GFP-CAR+) cells indicating transduction efficiency, proportion of CD4$^+$ and CD8$^+$ T cells, and expression of activation markers (CD25, PD1, and granzyme B (GzmB). (D) In vitro cytotoxic activity of CART3-mCALR cells from HD and patients against HEL mCALR$^+$ target cells at (left) 24 hours and (right) 48 hours, measured by luminescence-based assays (HD, n=3, patients n=5). (E) Cytotoxicity of autologous CART3-mCALR cells against primary CD34$^+$ malignant cells from patients. Left panel: representative images of bone marrow biopsies of patients (NH23060, NH25006) used in cytotoxicity. Up: hypercellular bone marrow with increased number of megakaryocytes forming dense clusters and displaying atypical morphology (cloud-like and hyperchromatic nuclei) H&Ex200. Down: reticulin stain grade 2 MF. Right panel: target cells were pre-labeled with eFluor and co-cultured with CAR T cells for 48 hours. Cell death was assessed by flow cytometry based on viable (eFluor$^+$ 7AAD$^-$) target cells and normalized to control co-cultures with non-transduced T cells. Data are presented as mean±SD. Statistical significance was determined using unpaired two-tailed Student's t-tests. ***p<0.001. E:T, effector-to-target; HD, healthy donor; mCALR, mutant calreticulin; MPN, myeloproliferative neoplasm.

(HSPCs) derived from peripheral blood CD34$^+$ cells of MPN patients (figure 6A). The cohort included patients with ET (n=7) and MF (n=12) (online supplemental table 3), carrying driver mutations in JAK2V617F (n=7), CALR (n=8), and MPL (n=4). Control samples corresponded to SRR30220813-16 from study SRP526030.

Principal component analysis revealed a clear clustering of MPN samples and a separation from healthy controls (online supplemental figure 11). Differential expression analysis indicated a distinct transcriptional profile, with several genes significantly up- or downregulated in patients compared with controls (figure 6A).

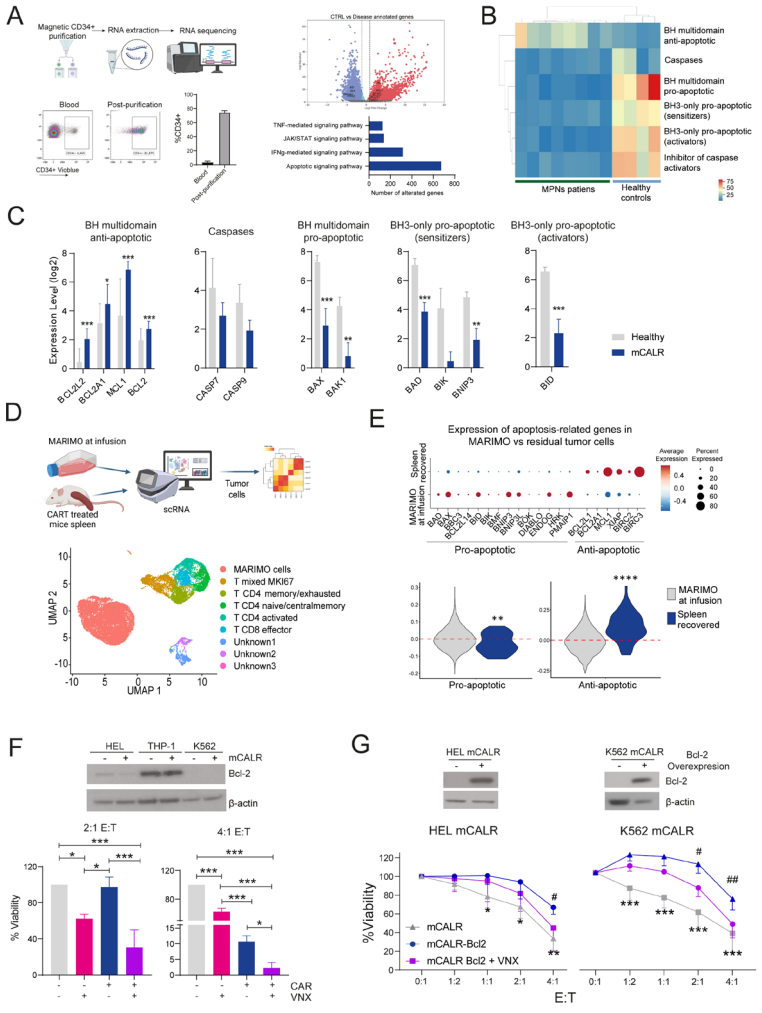

Figure 6 Dysregulation of mtApoptosis in MPN HSPCs underlies resistance to CAR T-cell therapy and is reversed by BH3-mimetics. (A) Upper left panel: schematic representation of the experimental workflow: RNA-seq was performed on CD34$^+$ HSPCs isolated from the peripheral blood of MPN patients. Lower left panel: representative dot plots of CD34 in blood and post-purification, and summary graph bar showing %CD34. Upper middle panel: volcano plot displaying differentially expressed genes between MPN patients and HD. Lower middle panel: functional enrichment analysis of differentially expressed genes, grouped by GO terms, KEGG pathways, and REACTOME annotations. (B) Heatmap graph showing the relative expression of mitochondrial apoptosis-related genes in CD34$^+$ from HD (blue line) and from mutated calreticulin-positive patients (mCALR, green line). (C) Relative gene expression clustered by functionality in HD (gray) and MPN CD34$^+$ HSPCs (blue). Statistical differences were assessed between mCALR patients and HD for each gene cluster. (D) Upper panel: Experimental workflow showing the analysis of Marimo tumorous cell and spleen samples from CART3-mCALR-treated mice by single-cell RNA sequencing (scRNA-seq). Lower panel: UMAP projection of all human cells identified in the spleen, illustrating distinct clusters corresponding to MARIMO tumor cells and multiple T-cell subsets. Clusters labeled as "Unknown1–3" correspond to minor subpopulations with heterogeneous transcriptional profiles that could not be confidently assigned to a specific lineage based on canonical markers. (E) Upper panel: Dot plot showing the expression of apoptosis-related genes in MARIMO cells before infusion ("MARIMO at infusion") and in residual tumor cells recovered from treated mouse spleens ("Spleen recovered"). Lower panel: Violin plots representing cumulative apoptotic (left) and anti-apoptotic (right) gene signature scores derived from the normalized expression of the indicated genes. Residual tumor cells show decreased pro-apoptotic and increased anti-apoptotic signatures ($p<0.01$ and $^{**}p<0.0001$, respectively; Wilcoxon test), confirming a shift toward an anti-apoptotic transcriptional state following in vivo CART3-mCALR exposure. (F) Upper: western blot analysis of Bcl-2 protein expression in leukemic cell lines (HEL, THP-1, and K562), including wild-type and mCALR variants. Lower panel: CART3-mCALR cells cytotoxicity against THP-1 mCALR$^+$ cells in the presence or absence of 2 µM venetoclax (VNX) at the indicated E:T ratio after 48 hours using a luminescence-based assay. Below each bar, conditions are annotated to indicate the presence or absence of CART3-mCALR cells and VNX. (G) Upper: western blot showing overexpression of Bcl-2 in HEL mCALR$^+$ and K562 mCALR$^+$ cell lines. Lower panel: CART3-mCALR cells cytotoxicity against the indicated cell line (HEL mCALR$^+$ and K562 mCALR$^+$) without Bcl-2 overexpression (gray), with Bcl-2 overexpression (blue), and Bcl-2 overexpression treated with VNX (purple) at different E:T ratios after 24 hours using a luminescence-based assay. *Statistical significance between gray and blue, # statistical significance between blue and purple. Data are presented as mean±SD (n=3). P values were calculated using unpaired two-tailed Student's t-tests. */#$p<0.05$, **/##$p<0.01$, ***$p<0.001$. E:T, effector-to-target; HD, healthy donor; HSPCs, hematopoietic stem and progenitor cells; MPNs, myeloproliferative neoplasms.

Functional enrichment analysis of differentially expressed genes identified significant alterations in key biological pathways. Grouping by Gene Ontology (GO) terms, KEGG pathways, and Reactome annotations highlighted dysregulation in pathways potentially implicated in resistance to CAR-T cell therapy. These pathways included IFN-γ signaling, TNF-α signaling, and, most prominently, the apoptotic signaling pathway (figure 6A).

Apoptosis emerged as one of the most highly dysregulated pathways in MPN. Resistance to apoptosis, particularly via the intrinsic mitochondrial pathway (mtApoptosis), is a well-established hallmark of hematologic malignancies, though its transcriptional profile in MPNs remains underexplored. The genes involved in mtApoptosis include members of the Bcl-2 family, categorized into three subgroups: pro-apoptotic effectors (eg, *BAX, BAK*), anti-apoptotic (eg, *BCL2, MCL1, BCL2L2*), and BH3-only proteins that act as activators or sensitizers of apoptosis, as well as caspases and their inhibitors. Focused analysis of the mtApoptosis pathway revealed consistent downregulation of pro-apoptotic genes and upregulation of anti-apoptotic genes, with a slight reduction in caspase expression (figure 6B). This pattern was observed in all MPN CD34$^+$ samples with CALR mutations. No significant differences were found between ET and MF subtypes or between mCALR and non-mCALR cases, suggesting that mtApoptosis dysregulation is a general feature of MPNs regardless of the driver mutation (online supplemental figure 12).

Notably, anti-apoptotic genes such as *BCL2L2, BCL2A1, MCL1*, and *BCL2* were significantly upregulated (figure 6C), while pro-apoptotic genes, including *BAX*, *BAK1*, *BID*, *BIK*, *BAD*, and *BNIP3*, were downregulated, along with reduced expression of *CASP7* and *CASP9*. These findings indicate a transcriptional shift toward cell survival in MPN HSPCs, consistent with apoptosis dysregulation as a hallmark of disease pathogenesis.

Given that mtApoptosis plays a key role in lymphocyte-mediated cytotoxicity,[34] its dysregulation may reduce the sensitivity of malignant clones to CAR-T cell therapy. To investigate whether this mechanism could contribute to therapy resistance, we performed single-cell RNA sequencing (scRNA-seq) of the MARIMO cell line used for infusion, and of spleen samples collected on euthanasia from treated mice (figure 6D). This analysis aimed to identify residual tumor cells and determine whether those surviving exhibited an apoptotic signature favoring resistance.

Single-cell RNA sequencing revealed distinct transcriptional landscapes. UMAP projection and clustering separated MARIMO tumor cells from human T-cell populations in the mouse spleen, showing transcriptional features associated with proliferative (*MKI67*$^+$) T cells, CD8 effector cells, CD4-activated cells, and CD4 naïve/central memory T cells. Dot plot visualization of representative genes for each cluster confirmed their lineage and functional identities within the T-cell compartment, as well as tumor-associated signatures in MARIMO cells (figure 6D and online supplemental figure 13).

Focusing on apoptosis-related programs, dot plot analysis revealed increased expression of anti-apoptotic genes (*MCL1*, *BCL2L1*, *BCL2A1*, *XIAP*, *BIRC2* [cIAP1], *BIRC3* [cIAP2]) and a concomitant downregulation of pro-apoptotic mediators (*BAX*, *BOK*, *BAD*, *BBC3* (PUMA), *PMAIP1* (NOXA), *BID*, *BIK*, *HRK*, *BMF*, *BNIP3*, *BNIP3L*, *BCL2L14*, *DIABLO*, *ENDOG*) in tumor cells recovered from treated mice. To capture these trends globally, we computed apoptotic and anti-apoptotic signature scores by summing the normalized expression of genes in each category across clusters. These cumulative analyses confirmed a shift toward an anti-apoptotic transcriptional state in MARIMO cells following in vivo exposure to CART3-mCALR cells (figure 6E).

Based on these observations, we next assessed whether pharmacologic inhibition of anti-apoptotic BCL-2 family members could restore CAR T-cell cytotoxicity. We assessed the expression of anti-apoptotic Bcl-2 family proteins (Bcl-2, Mcl-1, and BCL2L1/Bcl-xL) in the cell lines used as models to evaluate CAR-T cell activity. Of the three tested cell lines, only THP-1 cells showed elevated Bcl-2 expression. Pretreatment with the Bcl-2 inhibitor venetoclax enhanced the cytotoxic effect of CART3-mCALR cells, particularly at low E:T ratio, when CAR-T cell cytotoxicity was more limited (figure 6F).

Additionally, we overexpressed Bcl-2 in HEL mCALR$^+$ and K562 mCALR$^+$ cells, confirming that inhibiting the mtApoptosis pathway reduces CAR-T cell cytotoxicity at low E:T ratios (figure 6G). However, this resistance was effectively reversed by pretreatment with venetoclax, resulting in a synergistic enhancement of CAR-T cell activity in both Bcl-2 overexpressing cells. A similar effect was noted following the overexpression of other anti-apoptotic proteins (online supplemental figure 14), suggesting that the observed resistance is linked to the mtApoptosis pathway rather than to any single protein. Together, these findings identify mtApoptosis dysregulation as a potential mechanism of resistance to CART3-mCALR therapy and support the rationale for combining CAR T-cell therapy with BH3 mimetics to enhance eradication of mCALR-mutant clones in myeloproliferative neoplasms.

DISCUSSION

For the first time, we demonstrate the potential of targeting MPNs with CAR-T cell therapy directed against CALR mutations, a novel approach in an area where no cellular therapies are currently available. Using both in vitro systems with cell lines, patient-derived samples, and in vivo xenograft models, we show that the selected lead candidate exhibits high efficacy among all CAR constructs tested, even against cells with low antigen expression such as MARIMO cells. This suggests a capacity to eliminate malignant clones with reduced mCALR surface expression, a key finding considering the potential for antigen

escape in clinical settings. Beyond efficacy testing, we investigated resistance mechanisms based on common co-occurring mutations found in patient samples. Consequently, we propose combinatorial strategies to overcome resistance, which not only enhance therapeutic efficacy but could also serve as biomarkers to predict resistance. While promising, these findings require further validation in appropriate clinical cohorts.

Despite advances in MPN therapies over the last decade, outcomes for myelofibrosis remain poor.[35] Interest in incorporating CAR-T cells and other immunotherapies into MPN treatment has grown, but progress has been limited due to the challenge of identifying tumor-specific antigens.[25] The primary driver mutations in MPN affect three genes encoding two intracellular proteins (JAK2 and CALR) and the cell surface receptor TPOR/MPL.[36 37] However, *MPL* mutations predominantly occur in the transmembrane domain, making them unsuitable targets for immunotherapy.[38] In contrast, CALR mutations disrupt its ER retention signal (KDEL), resulting in aberrant localization on the plasma membrane, a process that has been shown to be mediated by MPL. However, as shown in our study and supported by previous data,[9 26] functional mCALR can be located on the plasma cell membrane by an MPL-independent mechanism that remains to be characterized.[13–15]

Four of the five CAR-T constructs tested showed in vitro activity, with CART3-mCALR demonstrating the most consistent efficacy across various cell lines. CART3-mCALR exhibited robust cytotoxicity against both MPL-expressing (HEL mCALR$^+$, THP-1 mCALR$^+$) and MPL-negative (K562 mCALR$^+$, MARIMO) cell lines. Notably, despite lacking MPL and having low levels of mCALR expression, MARIMO cells were effectively targeted by CART3-mCALR cells both in vitro and in vivo. It is important to note that detecting mCALR on the cell membrane remains technically challenging due to the unavailability of high-quality, commercially available antibodies. Even in cell lines engineered to overexpress mCALR, the surface expression levels identified by flow cytometry and immunoblotting were low. This limitation hindered the reliable quantification of mCALR surface levels in patient-derived samples. However, this technical constraint does not undermine the validity or potential of our conclusions, as functional assays using both mCALR-positive and mCALR-negative cell lines, including MARIMO, as well as primary patient samples, demonstrated specific and effective CAR-T cell-mediated targeting of mCALR-expressing cells. To improve detection capabilities in future studies, we have begun developing custom high-affinity scFvs against mCALR, which may enhance sensitivity for surface detection. Importantly, these tools are intended to support future work but are not essential for the functional validation and key findings presented here.

The in vivo cytotoxic effect in the MARIMO model was slightly lower than in the HEL mCALR$^+$ model when using a high tumor cell inoculation, which may be attributed to the faster engraftment and disease progression of MARIMO cells. This difference in growth kinetics was evident in the control groups: MARIMO-bearing mice succumbed around day 21, whereas HEL mCALR$^+$-bearing mice survived until day 28. Nevertheless, the primary objective of eliminating malignant clones from the bone marrow and spleen, the key compartments involved in MPN pathogenesis, was successfully achieved in both models, accompanied by CAR-T cell expansion. In addition, experiments using a lower dose of MARIMO cells, reflecting a slower growth similar to the initial phases of the disease in humans, demonstrated a high long-term efficacy of the CAR-T cells. Altogether, these results support the therapeutic potential of CART3-mCALR cells. One limitation of our in vivo model is that it does not fully recapitulate the interplay between CAR-T cells and the host immune system, a factor known to enhance CAR-T function and promote epitope spreading. The latter may be critical for improving the targeting of malignant clones and achieving broader disease control in MPNs, as demonstrated in a murine model where IFN-γ played a key role.[39]

The ability of CART3-mCALR cells to eliminate MARIMO cells, which express low levels of mCALR and lack MPL, challenges the prevailing model that associates mCALR surface expression with MPL-dependent mechanisms.[13 15] Our data using the MPL-negative cell line K562 further supports this result. This discrepancy may be explained by considering the broader functional roles of wild-type CALR. While wild-type CALR is primarily localized to the ER, where it facilitates glycoprotein folding and calcium homeostasis, it also exerts functions outside the ER, at the cell surface, where it regulates processes such as adhesion, coagulation, gene expression, and immune modulation. Therefore, mCALR may retain certain extracellular membrane-associated functions independent of MPL. It should be noted that, supporting our findings, other studies have shown functional MPL-independent mCALR activity in both cell-based and *C. elegans* models, suggesting that mCALR may interact with and activate cell surface receptors other than MPL.[26 27] Future studies should investigate potential interactions between mCALR and other surface proteins to determine whether such interactions contribute to MPN pathogenesis independently of the mCALR–MPL–JAK2–STAT5 signaling axis, for example, via MAPK signaling pathways.[13 27 40–42]

CART3-mCALR cells exhibited robust proliferation during tumor treatment, accompanied by high levels of activation and cytotoxicity both in vitro and in vivo. Additionally, they demonstrated a potent effector and central memory T-cell phenotype in vivo, which may contribute to long-lasting immune protection against relapse in high-risk patients.[32] Given the recurrence rate of myelofibrosis (10%–30%) following allogeneic hematopoietic cell transplantation (alloHCT), the sustained persistence of CART3-mCALR cells could be a key factor for the long-term success of CAR-T cell therapies targeting MPNs.[43] This hypothesis, however, will require

further experimental validation in appropriate preclinical models.

Importantly, we demonstrate that T cells from MPN patients can be successfully engineered into functional CAR-T cells that exhibit activation and cytotoxicity levels comparable to those derived from HDs, including the ability to eliminate mCALR$^+$ malignant clones in an autologous setting. This is a significant finding, considering the reported immune dysfunctions in MPN patients and the potential impact of prior treatments, such as ruxolitinib or chemotherapy, on T cell fitness.[6 44–46]

Our RNA-seq analysis of CD34$^+$ peripheral blood cells from MPN patients confirms the presence of apoptotic dysregulation in these neoplasms, showing overexpression of anti-apoptotic genes such as *BCL-2*, *BCLA1*, *BCL2L2*, *MCL-1*, and *BIRC3*, alongside reduced expression of pro-apoptotic genes, including the BH3-only proteins BID and BAD, as well as BAK and BAX. Disruption of these pathways may provide an additional mechanism of resistance. Consistent with this, our studies show that impaired intrinsic apoptotic signaling in tumor cells reduces CAR-T cell cytotoxicity and contributes to decreased efficacy, underscoring the critical role of apoptotic pathways in determining CAR-T cell effectiveness.[47–49] As expected, this is particularly relevant under conditions of limited CAR-T tumor interaction, such as low E:T ratios, conditions likely reflective of clinical scenarios. This aligns with prior evidence showing that mitochondrial apoptosis is essential for effective lymphocyte-mediated cytotoxicity, and that the apoptotic priming state of tumor cells influences their susceptibility to immune-mediated killing.[50 51] Indeed, our scRNA-seq analysis of residual tumor cells from CAR-T-treated mice showed an enrichment of cell populations that downregulate pro-apoptotic genes and overexpress anti-apoptotic ones, supporting our conclusion and highlighting the potential benefit of combining CAR-T therapy with drugs that modulate these pathways. This finding, although not the primary focus of this study, supports the potential use of apoptotic signaling molecules as biomarkers for predicting CAR-T cell response. Here, we demonstrate that co-treatment with sublethal doses of anti-apoptotic protein inhibitors effectively primes mtApoptosis in tumor cells, thereby enhancing the cytotoxic activity of CART3-mCALR cells. Combining BH3 mimetics with CART3-mCALR cells produced a synergistic killing effect on malignant clones.

Although there is currently limited evidence regarding the role of mtApoptosis dysregulation in the progression of MPN, it is known that these neoplasms frequently accumulate mutations beyond classical driver genes. Several of these mutations, including *ASXL1, TET2, DNMT3A, EZH2, IDH1/2, SRSF2, U2AF1*, and *TP53*, are linked to poor prognosis and often result in resistance to apoptosis by disrupting the balance between anti-apoptotic and pro-apoptotic proteins.[52–55] Notably, some apoptotic priming agents tested here that could enhance the efficacy of CART3-mCALR cells are already being evaluated in clinical trials for myelofibrosis patients with disease progression or suboptimal response to ruxolitinib monotherapy (ClinicalTrials.gov identifier: NCT03222609). Therefore, combining CART3-mCALR cells with agents that sensitize malignant clones to apoptosis may represent a promising therapeutic strategy, warranting further investigation in future preclinical and clinical studies.

Other research strategies have focused on antibodies targeting the mCALR neoepitope to inhibit mCALR-induced MPL signaling. INCA033989 is a novel human monoclonal IgG antibody currently in early clinical development for patients with mCALR-MF and ET.[24 36 56 57] However, the subcellular location where mCALR activates MPL is an important unresolved question. Although the mCALR–MPL complex is present at the cell surface, mCALR predominantly accumulates in the ER-to-Golgi intermediate compartment (ERGIC), where glycosylated proteins, including MPL, undergo maturation. It has been proposed that mCALR engages with MPL and triggers its premature activation within the ERGIC or other intracellular compartments during its trafficking to the cell surface.[25 58] As a result, the strategy of antibodies blocking MPL signaling at the cell surface may only have a partial effect since they might not be able to inhibit intracellular mCALR–MPL interactions.

In contrast, CAR-T cells targeting the mCALR neoepitope would have the capacity to eliminate all cells expressing mCALR. This approach could begin a new era of targeted therapy in MPNs.[57–60] Further safety testing, including broader reactivity studies using diverse cell lines, tissue libraries, and primary samples from healthy donors and patients, will be essential for clinical translation. Regulatory discussions will determine the extent of preclinical safety evaluations required for progression into clinical trials.

CONCLUSIONS

In conclusion, our study provides the first proof-of-concept that CAR-T cell therapy targeting mutant mCALR is a feasible and effective strategy for treating MPNs, a disease context where no cellular therapies are currently available. The demonstrated efficacy of our lead CAR-T candidate, even against cells with low antigen expression, suggests its potential to overcome antigen heterogeneity and minimize immune escape. Importantly, our identification of resistance mechanisms and corresponding combinatorial strategies improves therapeutic outcomes and opens avenues for the development of predictive biomarkers. These findings lay the groundwork for future clinical translation and suggest that mCALR-targeted CAR-T cells, particularly in combination with apoptosis-sensitizing agents, could offer a novel and personalized treatment modality for patients with mCALR MPNs. Future clinical trials will be essential to validate these results and define optimal patient selection strategies and combinatorial regimens.

MATERIAL AND METHODS

Patient-derived aberrant CD34+ cell cytotoxicity assays

Peripheral blood samples and data from patients diagnosed with MPNs were collected with the approval of the Clinical Research Ethics Committee of the Aragon Autonomous Community under code PI24/276. Diagnoses of PV, ET, and PMF were made according to the WHO's 2008 criteria and based on clinical and laboratory features. $CD34^+$ cells were enriched using magnetic-activated cell sorting (MACS) technology with the Miltenyi Biotec system. Briefly, PBMCs were obtained through density gradient centrifugation, incubated with CD34 MicroBeads (Miltenyi Biotec), and purified following the manufacturer's instructions. Isolated cells were cultured in StemSpan SFEM II Medium supplemented with StemSpanTM $CD34^+$ Expansion Supplement (STEMCELL Technologies) and hematopoietic cytokines (hSCF, hFLT3L, and hTPO (all from MiltenyiBio) at 100 ng/mL).

Target cells were labeled with 5 µM eFluor 670 (Invitrogen) and incubated with mCALR-CAR3 or no-transduced (NT) T cells at different E:T ratios for the indicated time periods. CART-mediated cytotoxicity was determined by counting the residual alive target cells (eFluor 670^+ $7AAD^-$) by using MACSQuant Analyzer 10 Flow Cytometer volumetric counting application and specific cell death was calculated with the following formula: % Specific death=(Number of alive target cells in co-culture with CART3-mCALR cells–Number of alive target cells in co-culture with NT T cells)/Number of alive target cells in co-culture with NT T cell×100.

Statistical analysis

All statistical analyses were conducted using GraphPad Prism V.8.0.1 or custom Python scripts employing the SciPy module for statistical computations. Briefly, t-tests were used for pairwise comparisons, and analysis of variance was used when comparing more than two groups. The Mantel-Cox log-rank test was used for survival curve analysis. Unless otherwise indicated in the figure legends, data are presented as mean±SD. A $p<0.05$ was considered statistically significant. To review the remaining Materials and Methods, please refer to online supplemental file 1.

Author affiliations
[1]Aragón Health Research Institute (IIS Aragón), Zaragoza, Spain
[2]CIBERINFEC, Carlos III Health Institute, Madrid, Spain, Spain
[3]Red RICOS de Terapias Avanzadas TERAV+, Carlos III Health Institute, Madrid, Spain
[4]CERTERA, Consorcio Estatal en Red para el desarrollo de Medicamentos de Terapias Avanzadas, Carlos III, Madrid, Spain
[5]Department of Microbiology, Pediatry, Radiology and Public Health, University of Zaragoza, Zaragoza, Spain
[6]Unidad de Nanotoxicología e Inmunotoxicología experimental, IIS Aragón, Zaragoza, Spain
[7]Universidad San Jorge de Zaragoza, Villanueva de Gállego, Spain
[8]Instituto de Investigación en Ingeniería de Aragón (I3A), Universidad de Zaragoza, Zaragoza, Spain
[9]Biamics, Servicios de Bioinformatica SL, Zaragoza, Spain
[10]Department of Mechanical Engineering, University of Zaragoza, Zaragoza, Spain
[11]Hematology Service, Miguel Servet University Hospital, Zaragoza, Spain
[12]Universidad de Zaragoza, Zaragoza, Spain
[13]Hematology Service, Lozano Blesa University Clinical Hospital, Zaragoza, Spain
[14]Institut d'Investigacions Biomèdiques August Pi i Sunyer (IDIBAPS), Barcelona, Spain
[15]Hematology Department, Barcelona Clinic University Hospital, Barcelona, Spain
[16]Facultat de Medicina, Universitat de Barcelona, Barcelona, Spain
[17]CSIC, Instituto de Carboquimica, Zaragoza, Spain
[18]ARAID, IIS Aragón, Zaragoza, Spain

Acknowledgements The authors would like to thank the Biobank of the Aragon Health System, integrated into the Spanish National Biobanks Network, as well as the scientific and technical staff of the Central Research Services of IACS, the University of Zaragoza and IISA, including the Flow Cytometry, Microscopy, Anatomy Pathology, Proteomics, Genomics, Medical Imaging and Phenotyping, Animal Core Facility and UNATI, for their collaboration. We are also grateful to Alba García from the Medical Imaging and Phenotyping Service, and to Laura Ordovás and Marina Ripalda for providing and characterizing human induced pluripotent stem cell-derived cardiomyocytes (hiPSC-CMs). We thank Dr. Lucía Ferrando Lamana (Department of Pathology, Lozano Blesa University Hospital, Zaragoza, Spain). We sincerely thank Pablo Menéndez for generously providing the third-generation lentiviral plasmids, Pedro Baptista for providing the HepG2 cells and Steffen Koschmieder and Yuichi Ishikawa for kindly supplying the MARIMO cells.

Contributors CP designed and performed experiments and wrote the first draft of the manuscript. MG-B, LSM, LS, LPA, NMM and JPB performed experiments. EI, EMG, JMG-A, DSM, EMG and MAA designed experiments and contributed to writing the manuscript. MA-V, FJR, EI and LG-M performed statistical analyses and analyzed RNA-seq data. BM-J, MTO, GAR, MG and AA-L selected patients, provided anatomical-pathological imaging at diagnosis, and contributed to manuscript writing. AR-L and JP conceived and designed the original study and experiments, wrote the manuscript, and are the guarantors. All authors reviewed and approved the final version of the manuscript. We used ChatGPT (OpenAI) and Grammarly to improve the quality of written English in the manuscript. These tools were employed exclusively for language refinement, such as grammar correction, sentence structure enhancement, and clarity of expression. They were not used to generate scientific content, analyze data, or draw conclusions.

Funding This work was funded by the Instituto de Salud Carlos III (ISCIII) through the Strategic Action in Health (AES), 2025 call, Health R&D Projects – Strategic Lines of Health Research (project/grant number: PI25/00236). AR-L is funded by a Ramón y Cajal contract (RYC2022-036627-I), financed by MCIN/AEI/10.13039/501100011033 and the European Social Fund (ESF) "Investing in your future" and ASPANOA. Grant PROY_B61_24 "proyectos de Investigación, desarrollo e innovación (I+D+i) en líneas prioritarias y de carácter multidisciplinar" funded by Gobierno de Aragón to AR-L and DSM. The Instituto de Salud Carlos III (ISCIII) through the Spanish Network of Advanced Therapies (RICORS/TERAV+), project RD24/0014/0015, and co-funded by the European Union (EU) to AR-L, JP, DSM and EMG. Work in the JP laboratory is funded by CIBERINFEC-ConsorcioCentro de Investigación Biomédica en Red- (CB21/13/00087), CERTERA andTERAV+ from Institutode Salud Carlos III, FEDER (Fondo Europeo de Desarrollo Regional),Gobierno deAragón (Group B29_23R, and LMP139_21), Grants PID2020-113963RBI00 andPID2024-157582OB-I00from MCIN/ AEI/10.13039/501100011033 and private social initiatives(FARO, AECC, Dona Médula, ASPANOA, and Carrera de la Mujer de Monzón No 101018587). Grant PID2022-136554OA-I00 funded by MICIU/AEI 10.13039/501100011033 and the European Regional Development Fund (ERDF)/EU to DSM. Predoctoral Grant for Ibero-Americas in Doctoral studies University of Zaragoza-Santander University (ACP), and Predoctoral Grant from AECC (CP). This work is part of a project that has received funding from the European Research Council (ICoMICS grant agreement No 101018587).

Disclaimer The funders had no role in the study design; in the collection, analysis, or interpretation of data; in the writing of the manuscript; or in the decision to submit the paper for publication.

Competing interests None declared.

Patient consent for publication Not applicable.

Ethics approval Samples and data from patients included in this study were provided by the Biobank of the Aragon Health System (National Registry of Biobanks B. B.0000873), integrated into the Platform ISCIII Biobanks and Biomodels (PT23/00146), and they were processed following standard operating procedures with the appropriate approval of the local Ethics and Scientific Committees (CEICA) (code PI24/276). All patient samples were collected and used after they signed the corresponding informed consent to participate. All animal procedures were approved by the Animal Experimentation Ethics Committee (code PI48/23). The care and use of animals were performed according to the Spanish Policy for Animal

Protection RD53/2013, which meets the European Union Directive 2010/63 on protecting animals used for experimental and other scientific purposes.

Provenance and peer review Not commissioned; externally peer reviewed.

Data availability statement Data are available in a public, open access repository. Data are available on reasonable request. All data relevant to the study are included in the article or uploaded as supplementary information. All data relevant to the study are included in the article and its supplementary information files. Bulk RNA sequencing data have been deposited in the European Nucleotide Archive (ENA) at the European Bioinformatics Institute (EMBL-EBI) under accession number PRJEB89437[61]. Single-cell RNA sequencing data have been deposited in the ENA under accession number PRJEB102810[62].

ORCID iDs
José Manuel Garcia-Aznar https://orcid.org/0000-0002-9864-7683
Julian Pardo https://orcid.org/0000-0003-0154-0730
Ariel Ramirez-Labrada https://orcid.org/0000-0002-3888-7036

REFERENCES

1 Loscocco GG, Guglielmelli P, Gangat N, *et al*. Clinical and molecular predictors of fibrotic progression in essential thrombocythemia: A multicenter study involving 1607 patients. *American J Hematol* 2021;96:1472–80.
2 Palandri F, Latagliata R, Polverelli N, *et al*. Mutations and long-term outcome of 217 young patients with essential thrombocythemia or early primary myelofibrosis. *Leukemia* 2015;29:1344–9.
3 Klampfl T, Gisslinger H, Harutyunyan AS, *et al*. Somatic mutations of calreticulin in myeloproliferative neoplasms. *N Engl J Med* 2013;369:2379–90.
4 Merlinsky TR, Levine RL, Pronier E. Unfolding the Role of Calreticulin in Myeloproliferative Neoplasm Pathogenesis. *Clin Cancer Res* 2019;25:2956–62.
5 Nangalia J, Massie CE, Baxter EJ, *et al*. Somatic CALR mutations in myeloproliferative neoplasms with nonmutated JAK2. *N Engl J Med* 2013;369:2391–405.
6 Holmström MO, Martinenaite E, Ahmad SM, *et al*. The calreticulin (CALR) exon 9 mutations are promising targets for cancer immune therapy. *Leukemia* 2018;32:429–37.
7 Holmström MO, Andersen M, Traynor S, *et al*. Therapeutic cancer vaccination against mutant calreticulin in myeloproliferative neoplasms induces expansion of specific T cells in the periphery but specific T cells fail to enrich in the bone marrow. *Front Immunol* 2023;14:1240678.
8 Ushijima Y, Ishikawa Y, Nishiyama T, *et al*. Clonal evolution process from essential thrombocythemia to acute myeloid leukemia in the original patient from whom the *CALR*-mutated Marimo cell line was established. *Nagoya J Med Sci* 2024;86:326–32.
9 Kollmann K, Nangalia J, Warsch W, *et al*. MARIMO cells harbor a CALR mutation but are not dependent on JAK2/STAT5 signaling. *Leukemia* 2015;29:494–7.
10 Guglielmelli P, Nangalia J, Green AR, *et al*. CALR mutations in myeloproliferative neoplasms: hidden behind the reticulum. *Am J Hematol* 2014;89:453–6.
11 Araki M, Yang Y, Imai M, *et al*. Homomultimerization of mutant calreticulin is a prerequisite for MPL binding and activation. *Leukemia* 2019;33:122–31.
12 Masubuchi N, Araki M, Yang Y, *et al*. Mutant calreticulin interacts with MPL in the secretion pathway for activation on the cell surface. *Leukemia* 2020;34:499–509.
13 Elf S, Abdelfattah NS, Baral AJ, *et al*. Defining the requirements for the pathogenic interaction between mutant calreticulin and MPL in MPN. *Blood* 2018;131:782–6.
14 Elf S, Abdelfattah NS, Chen E, *et al*. Mutant Calreticulin Requires Both Its Mutant C-terminus and the Thrombopoietin Receptor for Oncogenic Transformation. *Cancer Discov* 2016;6:368–81.
15 Papadopoulos N, Nédélec A, Derenne A, *et al*. Oncogenic CALR mutant C-terminus mediates dual binding to the thrombopoietin receptor triggering complex dimerization and activation. *Nat Commun* 2023;14:1881.
16 Pietra D, Rumi E, Ferretti VV, *et al*. Differential clinical effects of different mutation subtypes in CALR-mutant myeloproliferative neoplasms. *Leukemia* 2016;30:431–8.
17 Rotunno G, Pacilli A, Artusi V, *et al*. Epidemiology and clinical relevance of mutations in postpolycythemia vera and postessential thrombocythemia myelofibrosis: A study on 359 patients of the AGIMM group. *American J Hematol* 2016;91:681–6.
18 Rotunno G, Mannarelli C, Guglielmelli P, *et al*. Impact of calreticulin mutations on clinical and hematological phenotype and outcome in essential thrombocythemia. *Blood* 2014;123:1552–5.
19 Loscocco GG, Gesullo F, Capecchi G, *et al*. One thousand patients with essential thrombocythemia: the Florence-CRIMM experience. *Blood Cancer J* 2024;14:10.
20 Takenaka K, Shimoda K, Uchida N, *et al*. Clinical features and outcomes of patients with primary myelofibrosis in Japan: report of a 17-year nationwide survey by the Idiopathic Disorders of Hematopoietic Organs Research Committee of Japan. *Int J Hematol* 2017;105:59–69.
21 Hultcrantz M, Kristinsson SY, Andersson TM-L, *et al*. Patterns of survival among patients with myeloproliferative neoplasms diagnosed in Sweden from 1973 to 2008: a population-based study. *J Clin Oncol* 2012;30:2995–3001.
22 Hernández-Boluda JC, Pereira A, Kröger N, *et al*. Determinants of survival in myelofibrosis patients undergoing allogeneic hematopoietic cell transplantation. *Leukemia* 2021;35:215–24.
23 Cree IA. The WHO Classification of Haematolymphoid Tumours. *Leukemia* 2022;36:1701–2.
24 Reis ES, Buonpane R, Celik H, *et al*. Selective targeting of mutated calreticulin by the monoclonal antibody INCA033989 inhibits oncogenic function of MPN. *Blood* 2024;144:2336–48.
25 Tvorogov D, Thompson-Peach CAL, Foßelteder J, *et al*. Targeting human CALR-mutated MPN progenitors with a neoepitope-directed monoclonal antibody. *EMBO Rep* 2022;23:e52904.
26 Guijarro-Hernández A, Eder-Azanza L, Hurtado C, *et al*. Transcriptomic Analysis Reveals JAK2/MPL-Independent Effects of Calreticulin Mutations in a *C. elegans* Model. *Cells* 2023;12:186.
27 Kollmann K, Warsch W, Gonzalez-Arias C, *et al*. A novel signalling screen demonstrates that CALR mutations activate essential MAPK signalling and facilitate megakaryocyte differentiation. *Leukemia* 2017;31:934–44.
28 Pecquet C, Papadopoulos N, Balligand T, *et al*. Secreted mutant calreticulins as rogue cytokines in myeloproliferative neoplasms. *Blood* 2023;141:917–29.
29 Kagoya Y, Nakatsugawa M, Ochi T, *et al*. Transient stimulation expands superior antitumor T cells for adoptive therapy. *JCI Insight* 2017;2:e89580.
30 Bengsch B, Ohtani T, Khan O, *et al*. Epigenomic-Guided Mass Cytometry Profiling Reveals Disease-Specific Features of Exhausted CD8 T Cells. *Immunity* 2018;48:1029–45.
31 Sen DR, Kaminski J, Barnitz RA, *et al*. The epigenetic landscape of T cell exhaustion. *Science* 2016;354:1165–9.
32 Fraietta JA, Nobles CL, Sammons MA, *et al*. Disruption of TET2 promotes the therapeutic efficacy of CD19-targeted T cells. *Nature New Biol* 2018;558:307–12.
33 Blaeschke F, Stenger D, Kaeuferle T, *et al*. Induction of a central memory and stem cell memory phenotype in functionally active $CD4^+$ and $CD8^+$ CAR T cells produced in an automated good manufacturing practice system for the treatment of $CD19^+$ acute lymphoblastic leukemia. *Cancer Immunol Immunother* 2018;67:1053–66.
34 Pardo J, Wallich R, Martin P, *et al*. Granzyme B-induced cell death exerted by ex vivo CTL: discriminating requirements for cell death and some of its signs. *Cell Death Differ* 2008;15:567–79.
35 Alvarez-Larrán A, Angona A, Andrade-Campos M, *et al*. Cytoreductive treatment in patients with CALR-mutated essential thrombocythaemia: a study comparing indications and efficacy among genotypes from the Spanish Registry of Essential Thrombocythaemia. *Br J Haematol* 2021;192:988–96.
36 Achyutuni S, Nivarthi H, Majoros A, *et al*. Hematopoietic expression of a chimeric murine-human CALR oncoprotein allows the assessment of anti-CALR antibody immunotherapies in vivo. *Am J Hematol* 2021;96:698–707.

37 Guglielmelli P, Calabresi L. The MPL mutation. *Int Rev Cell Mol Biol* 2021;365:163–78.
38 Beer PA, Campbell PJ, Scott LM, *et al*. MPL mutations in myeloproliferative disorders: analysis of the PT-1 cohort. *Blood* 2008;112:141–9.
39 Alizadeh D, Wong RA, Gholamin S, *et al*. IFNγ Is Critical for CAR T Cell-Mediated Myeloid Activation and Induction of Endogenous Immunity. *Cancer Discov* 2021;11:2248–65.
40 Michalak M, Groenendyk J, Szabo E, *et al*. Calreticulin, a multi-process calcium-buffering chaperone of the endoplasmic reticulum. *Biochem J* 2009;417:651–66.
41 Gold LI, Eggleton P, Sweetwyne MT, *et al*. Calreticulin: non-endoplasmic reticulum functions in physiology and disease. *FASEB J* 2010;24:665–83.
42 Luo B, Lee AS. The critical roles of endoplasmic reticulum chaperones and unfolded protein response in tumorigenesis and anticancer therapies. *Oncogene* 2013;32:805–18.
43 Robin M, de Wreede LC, Wolschke C, *et al*. Long-term outcome after allogeneic hematopoietic cell transplantation for myelofibrosis. *Haematologica* 2019;104:1782–8.
44 Liu P, Zhao L, Loos F, *et al*. Immunosuppression by Mutated Calreticulin Released from Malignant Cells. *Mol Cell* 2020;77:748–60.
45 Tefferi A, Vaidya R, Caramazza D, *et al*. Circulating Interleukin (IL)-8, IL-2R, IL-12, and IL-15 Levels Are Independently Prognostic in Primary Myelofibrosis: A Comprehensive Cytokine Profiling Study. *JCO* 2011;29:1356–63.
46 Fan W, Cao W, Shi J, *et al*. Contributions of bone marrow monocytes/macrophages in myeloproliferative neoplasms with $JAK2^{V617F}$ mutation. *Ann Hematol* 2023;102:1745–59.
47 Dufva O, Koski J, Maliniemi P, *et al*. Integrated drug profiling and CRISPR screening identify essential pathways for CAR T-cell cytotoxicity. *Blood* 2020;135:597–609.
48 Yan X, Chen D, Wang Y, *et al*. Identification of NOXA as a pivotal regulator of resistance to CAR T-cell therapy in B-cell malignancies. *Signal Transduct Target Ther* 2022;7:98.
49 Catalán E, Jaime-Sánchez P, Aguiló N, *et al*. Mouse cytotoxic T cell-derived granzyme B activates the mitochondrial cell death pathway in a Bim-dependent fashion. *J Biol Chem* 2015;290:6868–77.
50 Pourzia AL, Olson ML, Bailey SR, *et al*. Quantifying requirements for mitochondrial apoptosis in CAR T killing of cancer cells. *Cell Death Dis* 2023;14:267.
51 Pan R, Ryan J, Pan D, *et al*. Augmenting NK cell-based immunotherapy by targeting mitochondrial apoptosis. *Cell* 2022;185:1521–38.
52 Tognon R, Gasparotto EP, Neves RP, *et al*. Deregulation of apoptosis-related genes is associated with PRV1 overexpression and JAK2 V617F allele burden in Essential Thrombocythemia and Myelofibrosis. *J Hematol Oncol* 2012;5.
53 McClatchy J, Strogantsev R, Wolfe E, *et al*. Clonal hematopoiesis related TET2 loss-of-function impedes IL1β-mediated epigenetic reprogramming in hematopoietic stem and progenitor cells. *Nat Commun* 2023;14:8102.
54 Bera R, Chiu M-C, Huang Y-J, *et al*. Genetic and Epigenetic Perturbations by DNMT3A-R882 Mutants Impaired Apoptosis through Augmentation of PRDX2 in Myeloid Leukemia Cells. *Neoplasia* 2018;20:1106–20.
55 Takei H, Coelho-Silva JL, Tavares Leal C, *et al*. Suppression of multiple anti-apoptotic BCL2 family proteins recapitulates the effects of JAK2 inhibitors in JAK2V617F driven myeloproliferative neoplasms. *Cancer Sci* 2022;113:597–608.
56 Benlabiod C, Psaila B. INCA033989: the first shot on goal for MPNs? *Blood* 2024;144:2278–9.
57 Available: https://clinicaltrials.gov/study/NCT06034002
58 Chachoua I, Pecquet C, El-Khoury M, *et al*. Thrombopoietin receptor activation by myeloproliferative neoplasm associated calreticulin mutants. *Blood* 2016;127:1325–35.
59 Available: https://clinicaltrials.gov/study/NCT05936359
60 Available: https://clinicaltrials.gov/study/NCT06150157
61 Ramírez-Labrada A, *et al*. Data from: bulk RNA sequencing analysis of mutant calreticulin–targeted CAR-T therapy models. European Nucleotide Archive (ENA), project PRJEB89437; 2025. Available: https://www.ebi.ac.uk/ena/browser/view/PRJEB89437
62 Ramírez-Labrada A, *et al*. Data from: single-cell RNA sequencing analysis of mutant calreticulin–targeted CAR-T therapy models. European Nucleotide Archive (ENA), project PRJEB102810; 2025. Available: https://www.ebi.ac.uk/ena/browser/view/PRJEB102810

Legends